

Trans-Golgi Network Localized ECHIDNA/Ypt Interacting Protein Complex Is Required for the Secretion of Cell Wall Polysaccharides in *Arabidopsis*^{OPEN}

Delphine Gendre,^{a,1} Heather E. McFarlane,^{b,1} Errin Johnson,^{a,2} Gregory Mouille,^c Andreas Sjödin,^{a,3} Jaesung Oh,^{a,4} Gabriel Levesque-Tremblay,^b Yoichiro Watanabe,^b Lacey Samuels,^b and Rishikesh P. Bhalerao^{a,5}

^aUmeå Plant Science Centre, Department of Forest Genetics and Plant Physiology, Swedish University of Agricultural Sciences, S-901 83 Umeå, Sweden

^bDepartment of Botany, University of British Columbia, Vancouver, British Columbia V6T 1Z4, Canada

^cInstitut Jean-Pierre Bourgin, Unité Mixte de Recherche 1318, Institut National de la Recherche Agronomique–AgroParisTech, Institut National de la Recherche Agronomique Centre de Versailles-Grignon, 78026 Versailles cedex, France

The secretion of cell wall polysaccharides through the *trans*-Golgi network (TGN) is required for plant cell elongation. However, the components mediating the post-Golgi secretion of pectin and hemicellulose, the two major cell wall polysaccharides, are largely unknown. We identified evolutionarily conserved YPT/RAB GTPase Interacting Protein 4a (YIP4a) and YIP4b (formerly YIP2), which form a TGN-localized complex with ECHIDNA (ECH) in *Arabidopsis thaliana*. The localization of YIP4 and ECH proteins at the TGN is interdependent and influences the localization of VHA-a1 and SYP61, which are key components of the TGN. YIP4a and YIP4b act redundantly, and the *yip4a yip4b* double mutants have a cell elongation defect. Genetic, biochemical, and cell biological analyses demonstrate that the ECH/YIP4 complex plays a key role in TGN-mediated secretion of pectin and hemicellulose to the cell wall in dark-grown hypocotyls and in secretory cells of the seed coat. In keeping with these observations, Fourier transform infrared microspectroscopy analysis revealed that the *ech* and *yip4a yip4b* mutants exhibit changes in their cell wall composition. Overall, our results reveal a TGN subdomain defined by ECH/YIP4 that is required for the secretion of pectin and hemicellulose and distinguishes the role of the TGN in secretion from its roles in endocytic and vacuolar trafficking.

INTRODUCTION

Cell elongation in plants requires the synthesis and remodeling of the rigid cell wall that encloses the plant cells. Primary cell wall consists of ~20 to 30% cellulose embedded in a matrix of soluble hemicellulosic and pectic polysaccharides with small amounts of structural and enzymatic proteins (reviewed in Sandhu et al., 2009; Carpita, 2011). While cellulose microfibrils are synthesized by plasma membrane (PM)-localized cellulose synthase complexes, pectins and hemicelluloses are synthesized at the Golgi apparatus (reviewed in Driouich et al., 2012).

¹ These authors contributed equally to this work.

² Current address: Sir William Dunn School of Pathology, University of Oxford, Oxford OX1 3RE, UK.

³ Current address: Division for CBRN (Chemical, Biological, Radiological, and Nuclear) Defence and Security, Swedish Defence Research Agency, Umeå, Sweden.

⁴ Current address: Centre for Plant Integrative Biology, University of Nottingham, Nottingham LE12 5RD, UK.

⁵ Address correspondence to rishi.bhalerao@slu.se.

The author responsible for distribution of materials integral to the findings presented in this article in accordance with the policy described in the Instructions for Authors (www.plantcell.org) is: Rishikesh P. Bhalerao (rishi.bhalerao@slu.se).

Some figures in this article are displayed in color online but in black and white in the print edition.

Online version contains Web-only data.

Articles can be viewed online without a subscription.

www.plantcell.org/cgi/doi/10.1105/tpc.113.112482

Polysaccharide-specific antibodies, mutants in polysaccharide biosynthesis, and protein glycosylation have revealed the sequence of cell wall polysaccharide biosynthesis on the distinct regions of the *cis*-, medial-, and *trans*-cisternae of the Golgi (Lynch and Staehelin, 1992; Zhang and Staehelin, 1992; Vicré et al., 1998; Chevalier et al., 2010). By contrast, the components involved in post-Golgi polysaccharide delivery to the cell wall remain poorly understood. Nevertheless, secretory vesicles emerging from the *trans*-Golgi network (TGN) contain cell wall components (Toyooka et al., 2009; Kang et al., 2011) and the vesicles number varies depending on secretion activity (Young et al., 2008). Furthermore, pharmacological inhibition of V-ATPase (VHA) activity at the TGN by Concanamycin A leads to secretory defects and related growth phenotypes (Dettmer et al., 2006; Brūx et al., 2008; Viotti et al., 2010). Those data strongly suggest that the TGN plays a central role in polysaccharide secretion. However, a lack of mutants defective in secretion of polysaccharide has limited our understanding of this process, and the molecular mechanisms mediating secretion to the cell wall remain largely unknown.

The TGN is a polymorphic tubular-vesicular network that matures from the *trans*-most cisternae of the Golgi stack (reviewed in Staehelin and Kang, 2008; Kang, 2011). Originally considered as an extension of the Golgi on the *trans*-side, recent data indicate that the TGN is actually a highly mobile organelle that can exist independently or in association with a Golgi or another TGN (Viotti et al., 2010). The primary function of the TGN

is to correctly pack and transport newly synthesized proteins and carbohydrates en route to vacuoles and the PM (reviewed in Richter et al., 2009). In animal cells, endocytosed material is received by the TGN from early endosome and recycling endosome (reviewed in De Matteis and Luini, 2008). By contrast, the plant TGN functions as the early endosome and directly receives material endocytosed from the PM (Dettmer et al., 2006; Viotti et al., 2010), increasing the complexity of the sorting required at the plant TGN. Moreover, while constantly receiving and secreting vesicles, the TGN must also regulate and maintain the proteins belonging to the intrinsic TGN machinery.

In recent years, knowledge of TGN morphogenesis and function in plants has increased dramatically, and several TGN components have been identified (Dettmer et al., 2006; Chow et al., 2008; Robert et al., 2008; Kang et al., 2011). Nevertheless, little is known about how the material destined for the endocytic, vacuolar, and secretory pathways is sorted at the TGN. In particular, the identity of the TGN components mediating secretion of cell wall material remains largely unknown (reviewed in Worden et al., 2012). We recently identified ECHIDNA (ECH), a protein required for TGN integrity and involved in secretion of unidentified cargo (Gendre et al., 2011). Here, we identified conserved proteins of the YIP (for YPT/RAB GTPase Interacting Protein) family in *Arabidopsis thaliana* that form a TGN-localized complex with ECH. We showed that the ECH/YIP complex is necessary for cell elongation and is required for the TGN-mediated secretion of cell wall polysaccharides, such as pectins. Importantly, the ECH/YIP complex does not play a role in vacuolar targeting and endocytosis. Thus, we identified the components of a post-Golgi trafficking mechanism that plays an important role in secretion, independently of the other TGN functions, such as endocytosis.

RESULTS

YIP4a and YIP4b Interact with ECH

To better understand the role of ECH (Gendre et al., 2011), we performed a yeast two-hybrid (Y2H) screen using ECH as bait against an *Arabidopsis* cDNA library (Hybrigenics). This screen identified two proteins from the YIP family encoded by the loci At2g18840 and At4g30260. These proteins were named YIP4a and YIP4b (previously referred to as YIP2; Drakakaki et al., 2011) based on their closest yeast homolog, YIP4p (YGL198W) (see Supplemental Figure 1A and Supplemental References 1 online). In *Arabidopsis*, seven proteins share the YIP domain. YIP4a and YIP4b are small proteins (30 kD) that exhibit 85% identity (see Supplemental Figure 1B online) and have five predicted transmembrane domains (see Supplemental Figure 1C online). YIP homologs in yeast and mammals interact with RAB GTPases and are involved in vesicle trafficking, but their functions are still poorly understood (Heidtman et al., 2003; Chen and Collins, 2005b, 2005a; Yoshida et al., 2008).

A two-by-two Y2H experiment confirmed that ECH and YIP4a/b interact (Figure 1A) and that YIP4a and YIP4b can hetero- and homodimerize. Importantly, the ECH and YIP4a/b interactions were validated in planta by coimmunoprecipitation (co-IP) assays (Figure 1B). These results clearly establish that

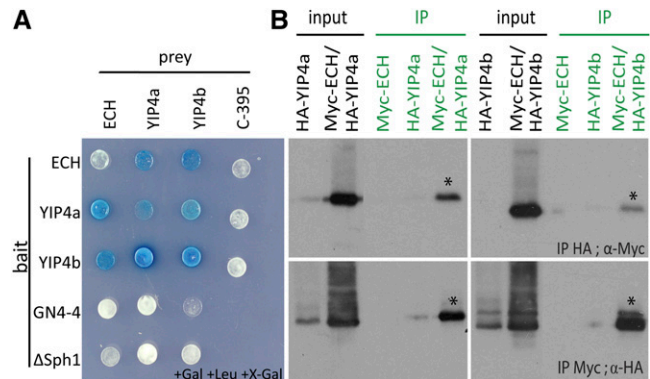


Figure 1. YIP4a and YIP4b Interact with ECH.

(A) Y2H assay between ECH, YIP4a, and YIP4b with C-395 and GN4-4 as negative interaction controls for prey and bait, respectively. To detect autoactivation of the prey constructs, a pEG202 derivative with a deleted *lexA* binding domain sequence (Δ Sph1; Grebe et al., 2000) was used as bait.

(B) Co-IP assay of Myc-ECH and HA-YIP4a or HA-YIP4b transiently expressed in *Arabidopsis* cell culture protoplasts. The top plots show the HA immunoprecipitation (IP), and the protein gel blot was performed using an anti-Myc antibody (α -Myc). The bottom plots show the results of the reciprocal experiment. Asterisks indicate interaction. [See online article for color version of this figure.]

ECH interacts with YIP4a and YIP4b either separately or with potential YIP4a/YIP4b dimers.

The *yip4a yip4b* Double Mutant Displays a Cell Elongation Defect

To understand the function of YIP4a and YIP4b, one T-DNA insertion line in the *YIP4b* gene (SALK_129888, *yip4b*) and two insertion lines in *YIP4a* (SALK_066428 and SALK_021897, *yip4a-1* and *yip4a-2*, respectively) were characterized. The insertion in *YIP4b* occurred in the second intron and generates a transcriptional knockout (see Supplemental Figure 2A online). The insertion in *yip4a-1* occurred at the beginning of the first intron of *YIP4a* and generates a truncated transcript, while the *yip4a-2* insertion occurs at the beginning of the 3' untranslated region (UTR) and does not affect the transcription of *YIP4a* (see Supplemental Figure 2A online). The phenotype of single *yip4* mutants was indistinguishable from the wild type (Columbia-0 [Col-0]) (Figure 2A). By contrast, *yip4a-1 yip4b* and *yip4a-2 yip4b* double mutants displayed clear growth defects (Figure 2A), suggesting that YIP4a and YIP4b act redundantly and are involved in growth regulation. The stronger phenotype for *yip4a-2 yip4b* over *yip4a-1 yip4b* was surprising because *yip4a-2* was not a transcriptional knockout. However, many studies have demonstrated the importance of UTRs for the stability and/or regulation of transcripts (Ortega et al., 2006 and reviewed in Gutiérrez et al., 1999), so the T-DNA insertion in the 3' UTR end of *YIP4a* may cause a drastic reduction in YIP4a protein level. The expression of either *YIP4a* or *YIP4b* driven by their respective endogenous promoters fully complemented *yip4a-2 yip4b* double mutants (Figure 2A), confirming that the *yip4a-2 yip4b* growth

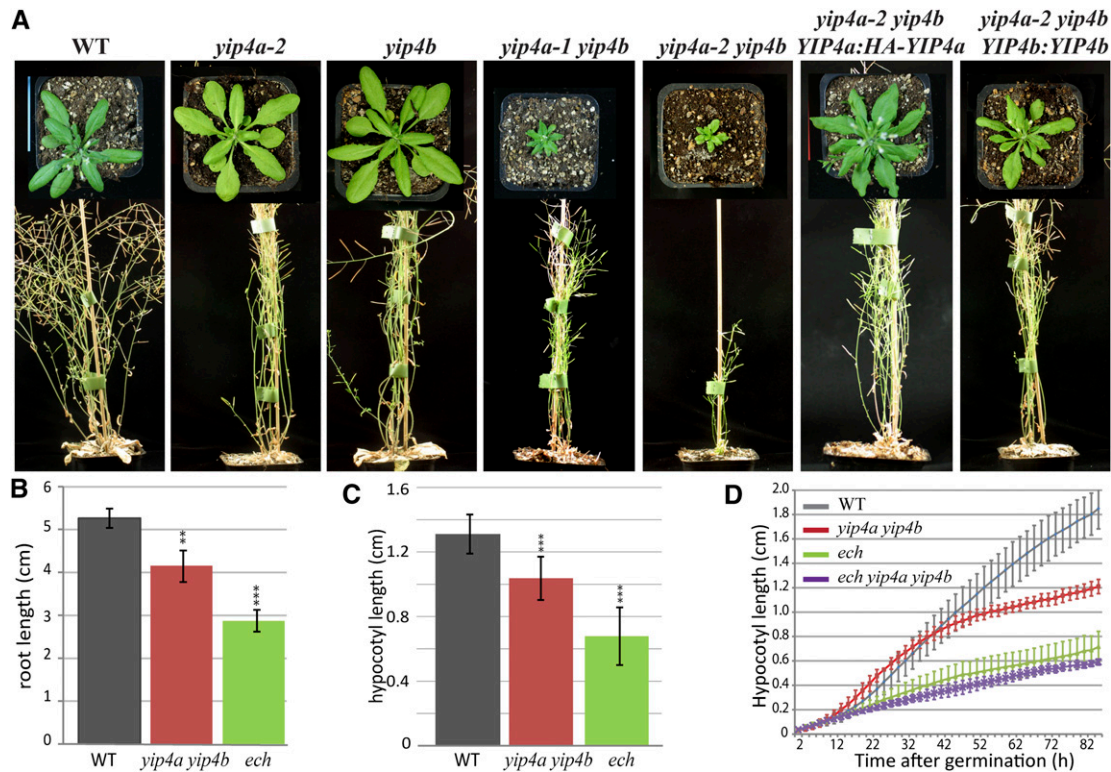


Figure 2. The *yip4a yip4b* Double Mutant Displays an Elongation Deficit.

(A) Five-week-old wild type (WT; Col-0), *yip4a-2* and *yip4b* single mutant, *yip4a-1 yip4b* and *yip4a-2 yip4b* double mutant, and *yip4a-2 yip4b* rescued by expression of YIP4a (HA N-terminal fusion) and YIP4b under their own promoter.

(B) Root length measurements of 10-d-old wild-type, *yip4a yip4b*, and *ech* seedlings grown in vitro (three replicates, each with 15 seedlings; average \pm sd).

(C) Etiolated hypocotyl length measurements of 5-d-old wild-type, *yip4a yip4b*, and *ech* seedlings grown in vitro in darkness (three replicates, each with 15 seedlings; average \pm sd).

(D) Etiolated hypocotyl growth kinematic of the wild type, *yip4a yip4b*, *ech*, and *ech yip4a yip4b* triple mutant ($n = 10$, average \pm sd). Significant differences are indicated as * $P < 0.05$, ** $P < 0.01$, and *** $P < 0.001$ (t test).

[See online article for color version of this figure.]

defect was due to the loss of function of the corresponding genes. Subsequent experiments were performed using the *yip4a-2 yip4b* double mutant, which is henceforth referred to as *yip4a yip4b*.

We then investigated hypocotyl and root elongation to better understand the growth defects in *yip4a yip4b*. The lengths of both 10-d-old seedling roots (Figures 2B; see Supplemental Figure 2B online) and 5-d-old dark-grown hypocotyls (Figures 2C; see Supplemental Figure 2C online) were 20% lower in *yip4a yip4b* than in the wild type. Since hypocotyl growth in darkness is due to cell elongation and not cell division (Gendreau et al., 1997), the growth reduction in *yip4a yip4b* suggests that YIP4a and YIP4b are required for cell elongation. While the exact reason for the less severe elongation phenotype of *yip4a yip4b* compared with *ech* is not known, this phenotype could potentially be due to other YIP4 related proteins substituting for the lack of YIP4, such as YIP5b, which also localizes to the TGN (Drakakaki et al., 2011).

The triple *ech yip4a yip4b* mutant displays an identical phenotype to *ech* with 50% length reduction, relative to the wild type, for both root (see Supplemental Figure 2D online) and

etiolated hypocotyl elongation (Figure 2D; see Supplemental Figure 2C online). In conjunction with the interaction data, the lack of additive effects in the triple mutant indicates that ECH and YIP4a/b act together to mediate a common step in cell elongation.

YIP4a and YIP4b Localize to the TGN

To better understand the function of the YIP4 proteins, the subcellular localization of YIP4a and YIP4b was investigated using N-terminal hemagglutinin (HA)-tagged YIP4a expressed under its native promoter and a specific YIP4b antibody (Figure 3B, inset). The HA-YIP4a fusion is functional, as shown by the successful rescue of the *yip4a yip4b* mutant (Figure 2A). YIP4a and YIP4b subcellular localisation were analyzed in root epidermal cells by colocalising anti-HA and anti-YIP4b signals with green, yellow or cyan fluorescent proteins (GFP, YFP, CFP) targeted to different organelles. G/Y/CFP fused to the Syntaxin of plant 61 (SYP61), V-ATPase subunit a1 (VHA-a1) and Rab GTPase A2a (RABA2a) are indicative of TGN localisation.

While the fluorescent proteins fused with *N*-acetylglucosaminyl transferase I (NAG1) and *N*- α -2,6-sialyltransferase (N-ST-YFP) are indicative of the Golgi. Both YIP4a (Figure 3A) and YIP4b (Figure 3B) signals strongly colocalized with TGN markers (Figures 3A and 3B; see Supplemental Figures 3A and 4A online), the highest colocalization is observed with SYP61-CFP (61% \pm 6.9% and 46.2% \pm 8.7%, respectively; Robert et al., 2008) and VHA-a1-GFP (64% \pm 10% and 38.9% \pm 6.5%; Dettmer et al., 2006) and to a lesser extent with fused to RABA2a-YFP (39% \pm 7% and 23.7% \pm 7.3%; Chow et al., 2008). By contrast, YIP4a and YIP4b signals displayed only minor colocalization with Golgi-localized proteins, such as NAG-EGFP (12% \pm 3.4% and 8.6% \pm 3.3%, respectively; see Supplemental Figures 3A and 3B online) and N-ST-YFP (10.7% \pm 3.7% and 18% \pm 3.6%; see Supplemental Figures 3A and 4F online), or with multivesicular body (MVB) markers, such as RABF2b-YFP (14% \pm 4.8% for YIP4a; see Supplemental Figure 3A online) and RABF1-GFP (5% \pm 2.4% for YIP4b; see Supplemental Figure 4C online). Importantly, a strong colocalization is observed between YIP4a and ECH antibody (60.4% \pm 9.4%; see Supplemental Figure 3A online), as well as YIP4b and ECH-YFP (38% \pm 7%; see Supplemental Figure 3B (38% \pm 7%; see Supplemental Figure 3B online). Moreover, YIP4a and YIP4b colocalized with each other as well (42.4% \pm 10.6% and 36% \pm 7% for the reverse; see Supplemental Figure 3A online). This confirms that the three proteins colocalize largely on the same TGN compartment (Figures 3A and 3B), in agreement with the protein-protein interaction between ECH and YIP4a/b.

Next we used treatment with Brefeldin A (BFA) and Wortmannin (Wm), two well-studied drugs affecting different steps in vesicle trafficking, to confirm the TGN localization of YIP4a and YIP4b. BFA affects trafficking mediated by some ARF GTPases (Jackson and Casanova, 2000) and results in a heterogeneous aggregation of TGN membrane encircled by Golgi apparatus in *Arabidopsis* root cells (Geldner et al., 2003; Lam et al., 2009; reviewed in Satiat-Jeunemaitre et al., 1996). Wm targets phosphatidylinositol kinases (Matsuoka et al., 1995) and causes fusion, swelling, and vacuolization of MVB in *Arabidopsis* root cells (Jaillais et al., 2008; Niemes et al., 2010). Thus, TGN and Golgi membranes would respond to a BFA treatment, while MVB membranes react to Wm. In accordance with the colocalization data, the majority of YIP4a and YIP4b signals accumulated in BFA bodies together with VHA-a1-GFP (Figures 3C and 3D, respectively) and was excluded from the Golgi (here labeled with N-ST-YFP; Figures 3E and 3F, respectively). Moreover, YIP4a and YIP4b compartments were mostly excluded from the characteristic ring-shaped bodies formed upon Wm treatment (here labeled with RABF1 or RabF2b) (see Supplemental Figure 3C online). Taken together, the colocalization data strongly support the localization of YIP4 proteins at the TGN with ECH.

The Localization of ECH and YIP4 at the TGN Is Interdependent

The colocalization of ECH and YIP4 and the interactions between these proteins prompted us to investigate whether the YIP4 proteins influence ECH localization at the SYP61/VHAA1 subdomain of the TGN and vice versa. To address this, we

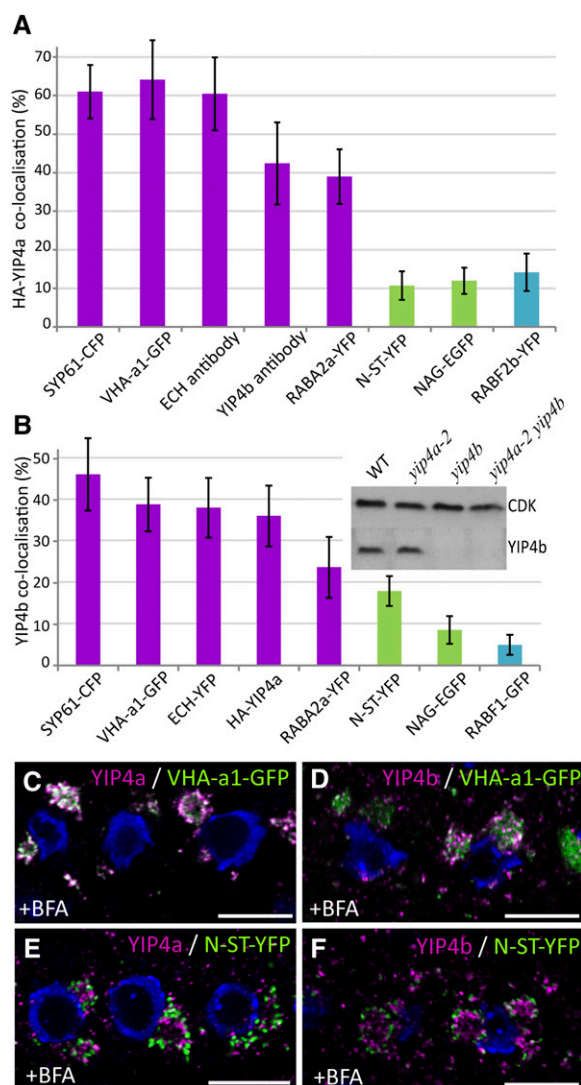


Figure 3. YIP4a and YIP4b Are TGN Localized.

(A) and (B) Quantitative measurement of colocalization of YIP4a (A) or YIP4b (B) with various markers. Markers of the TGN (magenta), Golgi apparatus (green), and MVB compartments (blue) are indicated by color coding. Quantification was achieved using the centroids method (Boutté et al., 2006) ($n = 10$ roots with four cells each; average \pm sd). The inset of the graph in (B) shows the specificity of the YIP4b antibody, which detected a single 30-kD band on protein gel blots only with protein extracts from the wild type (WT) and *yip4a-2*. CDK (cyclin-dependant kinase A) was used as a loading control.

(C) to (F) Colocalization between anti-HA (HA-YIP4a; [C] and [E]) or anti-YIP4b ([D] and [F]) labeling (magenta) and VHA-a1-GFP ([C] and [D]) or N-ST-YFP ([E] and [F]) after 1 h treatment with 50 μ M BFA. The 4',6-diamidino-2-phenylindole-stained nuclei are blue. Bars = 10 μ m.

investigated the colocalization of ECH and YIP4 proteins with the TGN markers SYP61 and VHA-a1 in *yip4a yip4b* and *ech* mutant backgrounds. In contrast with the wild type (Figures 4D to 4F), colocalizations of YIP4a or YIP4b with SYP61-CFP are significantly reduced in the *ech* mutant background by 30

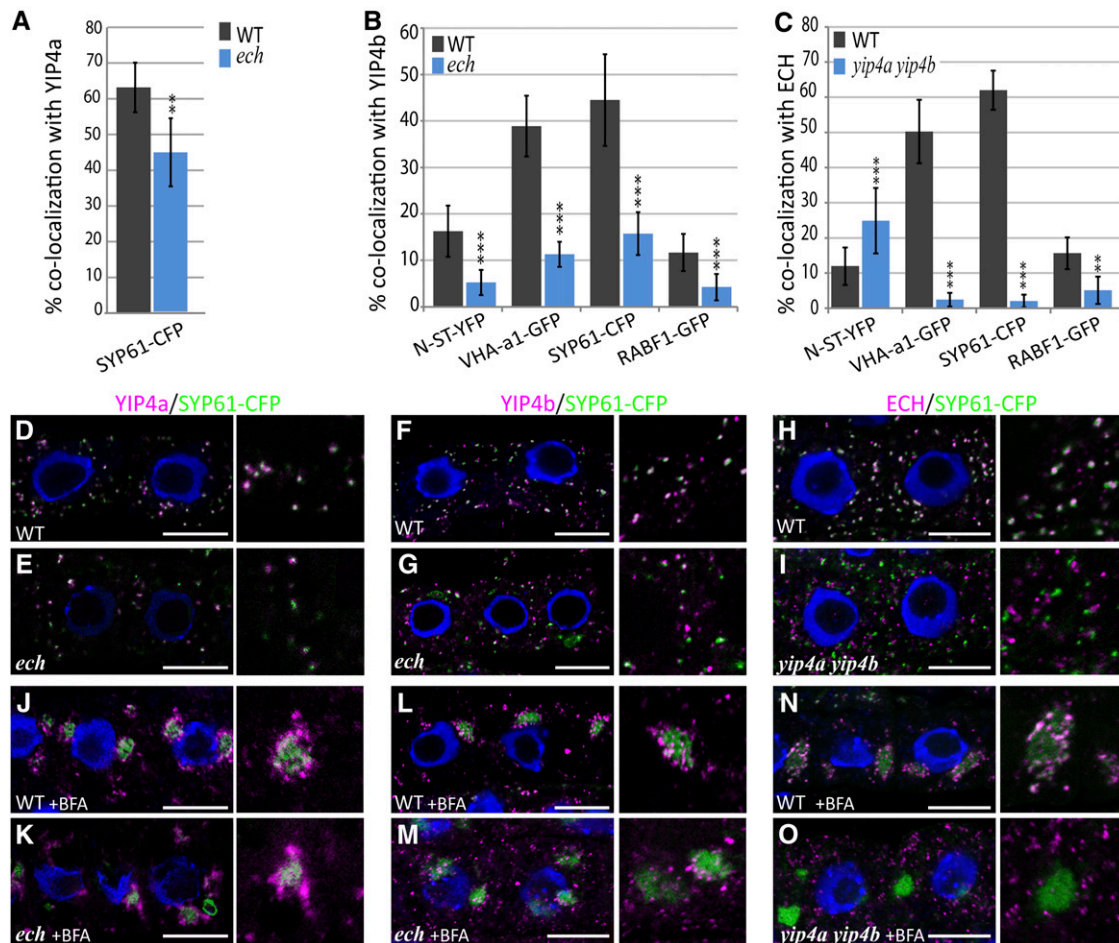


Figure 4. ECH, YIP4a, and YIP4b Are Dependent on Each Other for TGN Localization.

(A) to (C) Quantitative measurement of colocalization of YIP4a (A), YIP4b (B), or ECH (C) with various markers in wild-type (WT; gray bars) or mutant (blue bars) root epidermal cells ($n = 10$ roots with four cells, average \pm sd). Significant differences are indicated as * $P < 0.05$, ** $P < 0.01$, and *** $P < 0.001$ (t test).

(D) to (O) Representative images are displayed in Supplemental Figure 4 online and in (D) to (O) for colocalization with SYP61-CFP. Colocalization of anti-HA (YIP4a; [D], [E], [J], and [K]) anti-YIP4b ([F], [G], [L], and [M]) or anti-ECH ([H], [I], [N], and [O]) labeling (magenta) with SYP61-CFP (green) without treatment ([D] to [I]) or after 1 h treatment with 50 μ M BFA ([J] to [O]) in the wild type ([D] to [H]) and [J] to [N]) or mutant ([E] to [I]) and [K] to [O]). The 4',6-diamidino-2-phenylindole-stained nuclei are blue. Bars = 10 μ m.

and 65%, respectively (Figures 4A, 4B, and 4E to 4G). Strikingly, ECH colocalization with SYP61-CFP is drastically reduced by 96% in *yip4a yip4b* (Figures 4C and 4I) compared with the wild type (Figure 4H). Additionally, colocalizations of ECH or YIP4 with VHA-a1-GFP are also significantly reduced in the *yip4a yip4b* and the *ech* mutant background, respectively, compared with the wild type (Figures 4A to 4C; see Supplemental Figures 4A and 4B online). BFA treatment indicates that while SYP61-CFP still labeled BFA bodies in both the *yip4a yip4b* and *ech* mutant, YIP4a/b signal was reduced in BFA bodies in the *ech* mutant (Figures 4K to 4M). Similarly, ECH signals failed to localize to BFA bodies in the *yip4a yip4b* mutant (Figure 4O). Identical results were obtained with VHA-a1-GFP (see Supplemental Figures 4G and 4H online). These results further confirm that when YIP4 proteins

are not present, the TGN localization of ECH is disrupted and vice versa.

As ECH and YIP4 are depleted from SYP61/VHA-a1-positive TGN membranes, we then investigated which compartments they are mislocalized to in *yip4a yip4b* and *ech*. The absence of colocalization with RABF1b (Figures 4A and 4B; see Supplemental Figures 4C and 4D online) demonstrates that ECH and YIP4b are not mislocalized to MVBs in the *yip4a yip4b* and *ech* backgrounds, respectively. Interestingly, the ECH signal at the *trans*-Golgi cisternae (labeled by N-ST-YFP) is substantially increased in *yip4a yip4b* (Figures 4C; see Supplemental Figure 4F online), implying that some of the ECH signal could be retained in the *trans*-most Golgi cisternae in the absence of YIP4 proteins. Conversely, no such Golgi enrichment of YIP4b signal is found in *ech* (Figures 4B; see Supplemental Figure 4 online). Thus, our

data show that the TGN localization of ECH and YIP4 proteins is interdependent.

TGN Markers Are Partially Mislocalized in *yip4a yip4b*

We then investigated whether the TGN was altered by the loss of YIP4 proteins and made use of the known TGN resident proteins. In the *yip4a yip4b* mutants, SYP61-CFP was partially mislocalized to large ring-shaped compartments (Figure 5B) in

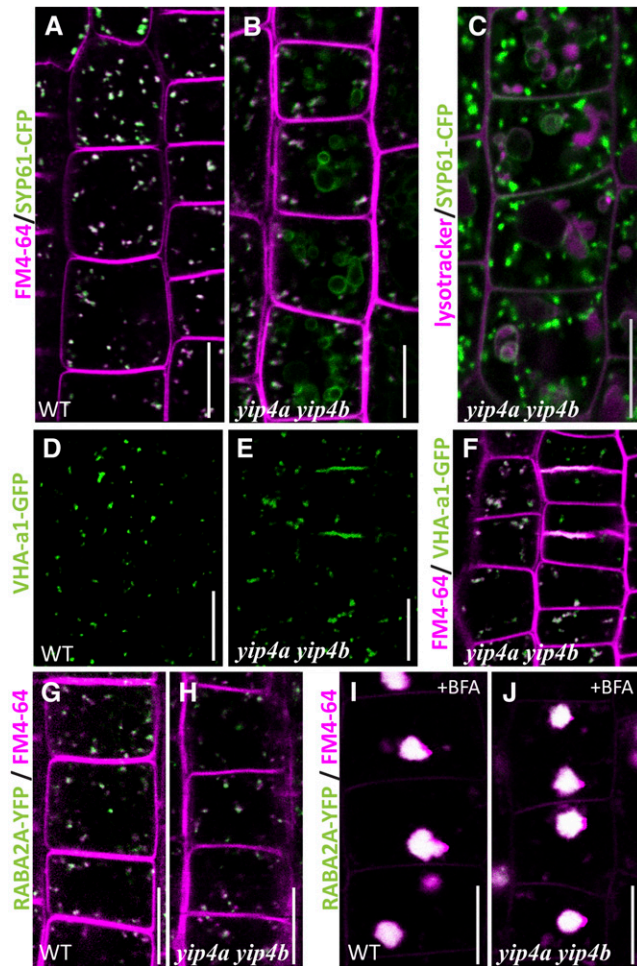


Figure 5. TGN-Localized Proteins Are Partially Mislocalized in *yip4a yip4b*.

(A) and (B) Colocalization between SYP61-CFP (green) and FM4-64 (magenta) after 5 min internalization in wild-type (WT) (A) and *yip4a yip4b* (B) root epidermal cells.

(C) Colocalization between SYP61-CFP and lysotracker red (50 nM, 30 min) in *yip4a yip4b*.

(D) and (E) VHA-a1-GFP labeling in wild-type (D) and *yip4a yip4b* (E) epidermal cells.

(F) Colocalization, in *yip4a yip4b*, of VHA-a1-GFP signal with FM4-64 after 5 min internalization.

(G) to (J) Colocalization of RABA2a-YFP with FM4-64 in untreated ((G) and (H)) or BFA-treated ((I) and (J)) wild-type ((G) and (I)) and *yip4a yip4b* seedlings ((H) and (J)). Bars = 10 μ m.

addition to the small punctate compartments observed in the wild type (Figure 5A). Lysotracker, which probes acidic organelles, indicated that those ring-shaped compartments are of lytic nature and therefore may be vacuoles (Figure 5C). Similarly, VHA-a1-GFP signal was more diffuse in *yip4a yip4b* cells than in the wild type (Figure 5D) and was also partly mislocalized to the cell plates (Figure 5E). Interestingly, RabA2a-YFP, a TGN protein residing on a domain partly distinct from SYP61/VHAA1 (Chow et al., 2008), is not mislocalized in *yip4a yip4b* (Figures 5G and 5H).

Although SYP61-CFP and VHA-a1-GFP are partially mislocalized in *yip4a yip4b*, the residual punctate signal is found in the core of BFA bodies following BFA treatment (Figure 4O; see Supplemental Figure 4H online), as described for the wild type (Figures 3C, 3D, and 4N; Geldner et al., 2003; Dettmer et al., 2006; Lam et al., 2009; Viotti et al., 2010). Furthermore, SYP61-CFP and VHA-a1 puncta colocalizes with FM4-64 within 5 min in the *yip4a yip4b* mutant (Figures 5B and 5F), revealing that those compartments still act as early endosome. These results indicate that a functional SYP61/VHAA1 TGN subdomain still exists in the *yip4a yip4b* mutant.

TGN-Golgi Association Is Affected by the Lack of YIP4 Proteins

As the TGN originates from the *trans*-most cisternae of the Golgi bodies (Staelin and Kang, 2008), we next investigated the TGN-Golgi association in the *yip4a yip4b* mutant. Confocal images indicate that neither Golgi bodies nor MVBs are affected, as the N-ST-YFP and RABF1-GFP signals remain unchanged in the *yip4a yip4b* double mutant (see Supplemental Figures 4D and 4F online). Transmission electron microscopy of the Golgi confirmed that the mean cisternal length is not affected in *yip4a yip4b* mutants compared with the wild type (see Supplemental Figure 5A online). The main difference observed between wild-type and *yip4a yip4b* cells was that fewer Golgi stacks have an associated TGN in *yip4a yip4b* compared with the wild type (see Supplemental Figure 5B online), as has been observed in the *ech* mutant (Gendre et al., 2011).

The YIP4a/YIP4b/ECH Complex Does Not Play a Role in Endocytosis or Vacuolar Transport

The mislocalization of TGN-resident proteins in *yip4a yip4b* and the dramatic growth phenotypes of these plants prompted us to investigate whether endocytosis, vacuolar trafficking, and/or secretion were perturbed. We investigated the potential effects on the endocytic pathway using FM4-64, a lipophilic dye that initially labels the PM and then every compartment traversed by the endocytic cargo before it reaches the tonoplast (Bolte et al., 2004). FM4-64 internalization followed the same time course in *yip4a yip4b* cells as in wild-type cells, staining the first endosomes within 5 min and reaching the tonoplast within 3 to 4 h (see Supplemental Figure 6A online). This suggests that the endocytic machinery is not impaired in *yip4a yip4b* mutants.

Furthermore, as both VHA-a3-GFP (Dettmer et al., 2006) and γ -TIP-GFP (Boursiac et al., 2005) labeled the tonoplast with equal intensity in the wild type and *yip4a yip4b* (see Supplemental Figure 6B online), vacuolar trafficking of membrane proteins is

unaffected by the loss of the YIP4 proteins. However, *yip4a yip4b* did exhibit some defects in vacuolar morphology similar to those described for *ech* (Gendre et al., 2011). Nevertheless, the soluble vacuolar cargo aleurain-GFP, which is known to use a vacuolar transport pathway distinct from γ -TIP-GFP (Gomez and Chrispeels, 1993), is correctly targeted to the main lytic vacuole in *yip4a yip4b* (see Supplemental Figure 6C online). In conclusion, the loss of YIP4 proteins does not affect endocytosis or transport to vacuolar cargo from the TGN.

The YIP4a/YIP4b/ECH Complex Is Required for Cell Wall Polysaccharide Secretion

In plants, cell elongation requires the biosynthesis of cell wall components, including pectins and hemicellulose, which are proposed to be delivered to the cell wall via TGN (reviewed in Carpita, 2011; Driouich et al., 2012). The cell elongation defects in the *ech* and *yip4a yip4b* mutants, along with the TGN localization of ECH and YIP4, prompted us to investigate whether the complex could be involved in secretion of soluble cell wall polysaccharides (pectin and hemicellulose) via TGN. The pectic matrix is structurally complex, featuring homogalacturonan, rhamnogalacturonan I (RGI), and rhamnogalacturonan II. Antibodies, including anti-RGI (LM5; Figure 6A), antimethylesterified homogalacturonan (JIM7; Figure 6B), and antixyloglucan (CCRC-M1; Figure 6C), labeled the cell wall of the wild-type, *ech*, and *yip4a yip4b* dark-grown hypocotyls. However, labeled pectin and xyloglucan also accumulated inside the *ech* and *yip4a yip4b* mutant cells (Figures 6A to 6C), which is never found in the wild type (Figure 6A, left panel). The most drastic intracellular polysaccharide accumulations were observed for LM5 (Figure 6A) and CCRC-M1 (Figure 6C), suggesting that the secretion of xyloglucan and RGI pectins are equally affected in *ech* and *yip4a yip4b*.

We further confirmed the defects in polysaccharide secretion by investigating the seed coat epidermis, in which the TGN is highly specialized for pectic mucilage secretion (Young et al., 2008). Ruthenium red staining of mucilage released from mature seeds was greatly reduced in both *yip4a yip4b* and *ech* seeds, relative to the wild type (Figure 7A). Sections through the seed coat that were stained with Toluidine Blue (Figure 7B) or labeled with the antimucilage antibody CCRC-M36 (Figure 7C; Young et al., 2008) revealed that *yip4a yip4b* and *ech* mucilage secretory cells display aberrant pectin localization. In the wild type, Toluidine Blue and CCRC-M36 strongly label the mucilage pockets situated at distinct apical domains of the secretory cells. In both the *yip4a yip4b* and *ech* mutants, Toluidine and M36 signal mainly labeled the center of the cell (Figures 7B and 7C), probably in the vacuolar lumen, with some signal also detected at the apoplastic mucilage pockets. Taken together, these data confirm that cell wall matrix polysaccharides, including both hemicelluloses and pectins, are not properly secreted and instead accumulate within *ech* and *yip4a yip4b* mutant seed coat cells and hypocotyls.

The defects in the secretion of cell wall components in *ech* and *yip4* mutants should result in alterations in the cell walls in these mutants. Therefore, we analyzed cell wall composition in the hypocotyls of etiolated *ech* and *yip4a yip4b* seedlings using Fourier transform-infrared (FT-IR) microspectroscopy, a powerful

method for identifying changes in the cell wall composition (Mouille et al., 2003). FT-IR analysis demonstrated that the cell walls of *ech*, *yip4a-1 yip4b*, and *yip4a-2 yip4b* are similar to one another, indicating similar cell wall defects in these mutants and that they are distinct from the wild type (see Supplemental Figure 7 online). Moreover, *ech* and *yip4a yip4b* generally cluster closer to mutants defective in soluble polysaccharides synthesis. Thus, these results indicate that the ECH/YIP4 complex is important for the TGN-mediated secretion of cell wall components such as pectins and xyloglucan, which ultimately affect cell wall composition. Interestingly, the secretion defect observed with polysaccharides is not a general secretion defect, as the PM proteins PIN2- and PIN3-GFP did not accumulate inside *yip4a yip4b* cells and are found at similar intensity levels at the PM of *yip4a yip4b* compared with the wild type (see Supplemental Figure 8 online).

DISCUSSION

Here, we show that the evolutionarily conserved ECH/YIP4 complex acts at the TGN to mediate the secretion of cell wall polysaccharides without affecting either endocytic or vacuolar trafficking in *Arabidopsis*. Secretion via the TGN plays a key role in cell elongation, as revealed by the impairment of cell elongation when TGN function is altered in the *ech* and *yip4a yip4b* mutants

ECH/YIP4a/YIP4b Is a Conserved Eukaryotic Interaction

We identified two members of the YIP domain family, YIP4a (At2g18840) and YIP4b (At4g30260), as interactors of ECH at the TGN. The similarities between *ech* and *yip4a yip4b* mutant phenotypes and the genetic, biochemical, and cell biological data indicate that ECH and YIP4a/YIP4b form a TGN-localized complex. Furthermore, YIP4 proteins are required for the maintenance of ECH on SYP61-VHA-a1-positive TGN compartments, and YIP4a and 4b rely at least partly on ECH for localization to this specific subdomain. Proteins of the YIP family are found in all eukaryotic organisms but have been studied most extensively in yeast and, more recently, in mammals. YIPs play a crucial role in vesicle trafficking (Yang et al., 1998; Matern et al., 2000; Barrowman et al., 2003; Heidtman et al., 2003; Chen et al., 2004; Chen and Collins, 2005b, 2005a; Yoshida et al., 2008; Kano et al., 2009; Tanimoto et al., 2011), which may involve their ability to bind RAB GTPases (RABs; hence their name Ypt/Rab Interacting Protein) (Yang et al., 1998), making them attractive candidates for the recruitment of RABs onto target membranes (Yang et al., 1998; Barrowman et al., 2003; Calero et al., 2003; Heidtman et al., 2003; Chen et al., 2004). YIP1p, the best characterized member of the yeast YIP family, acts in the secretory pathway at an early stage (Yang et al., 1998; Matern et al., 2000; Calero et al., 2003), but it remains unclear whether YIP1p regulates vesicle fusion at the Golgi apparatus (Barrowman et al., 2003) or vesicle budding from the endoplasmic reticulum (ER) (Heidtman et al., 2003). While YIP1p acts at the ER-Golgi interface, the other yeast YIPs, YIP4p and YIP5p, may function later in the secretory pathway (Inadome et al., 2007). *Arabidopsis* YIP4a and YIP4b display the YIP domain topology (Shakoori

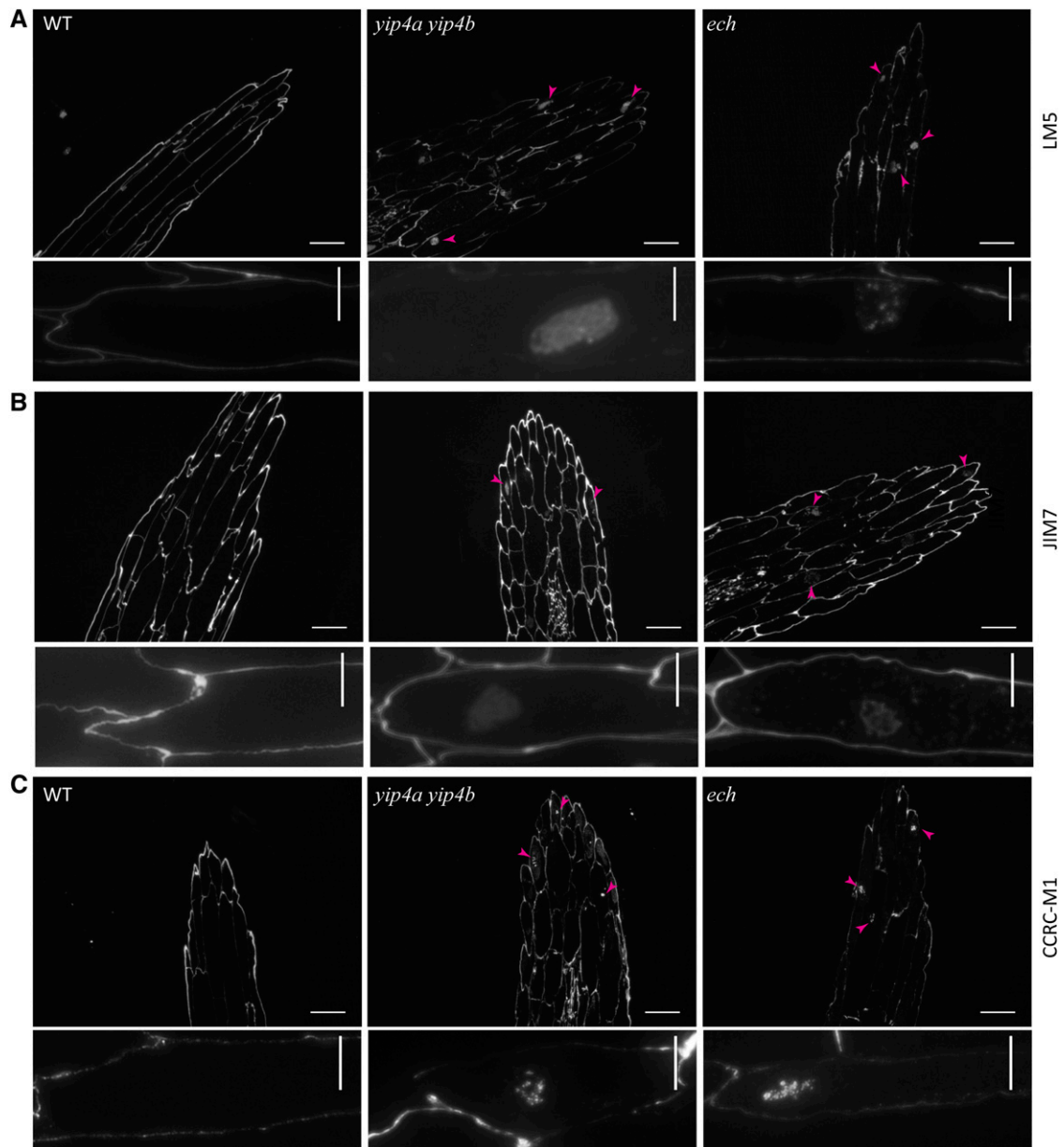


Figure 6. Intracellular Accumulation of Pectin and Xyloglucan in Dark-Grown Hypocotyls of *ech* and *yip4a yip4b*.

Wild-type (WT), *yip4a yip4b*, and *ech* etiolated hypocotyls immunolabeled with LM5 (**A**), JIM7 (**B**), or CCRC-M1 (**C**). Arrowheads indicate intracellular accumulation. Bars = 100 μ m; bars = 10 μ m in close-up images in bottom rows.

[See online article for color version of this figure.]

et al., 2003) and are most similar to yeast YIP4p. Like *Arabidopsis* YIP4 proteins, yeast YIP4p interacts with TVP23p, the yeast ortholog of ECH (Gendre et al., 2011), as demonstrated by Y2H (Uetz et al., 2000; Ito et al., 2001) and co-IP (Inadome et al., 2007). Moreover, ECH and YIP4 localizations are also conserved across species, as both TVP23p and YIP4p localize to the late Golgi/early endosome (Inadome et al., 2007), which corresponds to the plant TGN. Thus, ECH and YIP4a/b localizations and interaction have been conserved through evolution between the organisms

as distant as yeast and plants, indicating their functional importance for vesicle trafficking.

The ECH/YIP4a/YIP4b Interaction Is Important for TGN Maintenance and Function

Although the ECH (TVP23)/YIP4 interaction is evolutionarily conserved from yeast to plants, little was previously known about its role and function at the TGN in any organism partly due

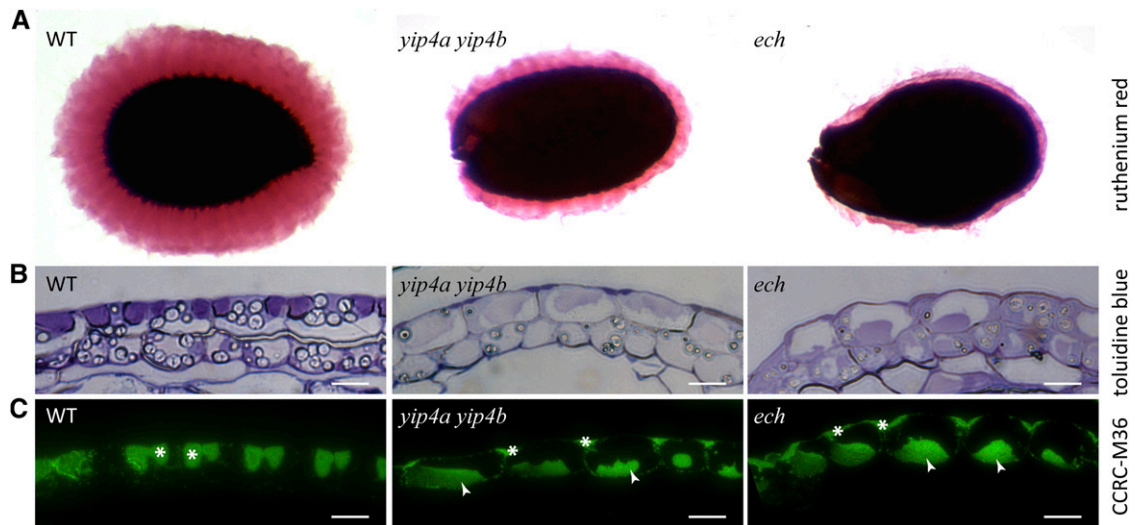


Figure 7. Intracellular Accumulation of Pectin Mucilage in *ech* and *yip4a yip4b* Seed Coats.

(A) Ruthenium red-stained seed coat mucilage after imbibition of wild-type (WT), *yip4a yip4b*, and *ech* seeds.

(B) and **(C)** Wild-type, *yip4a yip4b*, and *ech* seed coat sections stained with Toluidine Blue **(B)** or immunolabeled with CCRC-M36 **(C)**. Arrowheads indicate intracellular accumulation, and asterisks indicate mucilage pockets. Bars = 10 μ m.

[See online article for color version of this figure.]

to the lack of easily detectable phenotypes for the corresponding mutants. For example loss of yeast TVP23 or YIP4 has no measurable effect on growth (Calero et al., 2002; Stein et al., 2009). Nevertheless, when investigated, YIP proteins have been shown to be important for the maintenance and function of the compartments to which they localize. For example, in HeLa cells, YIPF3, YIPF4 (Tanimoto et al., 2011), and YIPF5 (Yoshida et al., 2008) are *cis*-Golgi located, and their loss leads to a partial fragmentation of the Golgi apparatus. We did not detect such defects in *ech* or *yip4a yip4b* mutants; instead, less TGN was associated with the Golgi in these mutants.

All YIP family members described so far in yeast and mammalian systems are Golgi located and are involved in ER-to-Golgi (Barrowman et al., 2003; Heidtman et al., 2003; Jin et al., 2005; Tanimoto et al., 2011) or Golgi-to-ER (Kano et al., 2009) transport. In *Arabidopsis*, the partial mislocalization of SYP61-CFP and VHA-a1-GFP in the absence of ECH (Gendre et al., 2011) or YIP4 proteins (this work) indicates that the ECH/YIP4 complex plays a key role in the maintenance of the TGN. Interestingly, in contrast with ECH, the loss of YIP4 does not lead to the mislocalization of RABA2a-YFP, which defines a subdomain of TGN that only partially overlaps the SYP61/VHAA1 domain (Chow et al., 2008). This suggests that ECH/YIP4 complex function could be restricted more specifically to the VHAA1/SYP61 subdomain.

We previously proposed that the TGN defects in *ech* (i.e., VHA-a1 and SYP61 partial mislocalization) could explain the growth/secretion defects (Gendre et al., 2011), as inhibition of V-ATPase activity with Concanamycin A mimics the *ech* and *yip4a yip4b* phenotypes. In *yip4* double mutants, VHA-a1-GFP localization is less affected than in *ech*, which correlates with the reduced severity of the *yip4a yip4b* double mutation on cell

elongation and mucilage secretion compared with *ech*. The localization of SYP61-CFP is also greatly affected by the absence of the ECH/YIP4a/YIP4b complex. Low levels of SYP61-CFP are often observed on the PM; recently, proteomic analysis of SYP61 compartments revealed that they may have a role in secretion (Drakakaki et al., 2011). The mislocalization of SYP61-CFP could thus be another factor that contributes to the phenotypes of *ech* and *yip4a yip4b*. However, the cell biological phenotypes of *syp61* loss-of-function mutants have not been described; therefore, the extent to which loss of SYP61 from TGN contributes to the *ech* and *yip4a yip4b* phenotypes remains to be seen.

The ECH/YIP4a/YIP4b Complex Defines a TGN Subdomain Mediating Polysaccharide Secretion

The ECH/YIP4 complex plays a key role in TGN maintenance since its absence leads to mislocalization of key components, such as VHA-a1, from the TGN. Since the TGN is a hub for several trafficking pathways, the defects in TGN could perturb any of the functions of the TGN, including vacuolar trafficking, endocytosis, and/or secretion. However, neither the endocytic nor the vacuolar route is affected in *ech* and *yip4a yip4b*. Instead, the secretion of cell wall polysaccharides is perturbed, as demonstrated by the intracellular accumulation of pectin and xyloglucan within *ech* and *yip4a yip4b* etiolated hypocotyl cells. This result explains the altered cell wall composition of the mutants revealed by FT-IR analysis and may underlie the cell elongation defects observed in both *ech* and *yip4a yip4b*. Furthermore, the seed coat phenotype of the *yip4a yip4b* and *ech* provides a rare opportunity to observe the perturbation of pectin traffic during a developmental period of abundant pectin

secretion. The loss of ECH or YIP4a/b leads to ineffective pectin transport to the seed coat mucilage pockets, resulting in almost no mucilage release from seeds upon hydration. Thus, the data from the seed coat analysis, together with that from hypocotyls, strongly support the role of ECH/YIP4 complex in secretion of pectin and xyloglucan via TGN.

Pectin and xyloglucan are important for cell elongation and play a key role in determining the mechanical properties of the cell walls. Changes in pectin and xyloglucan are associated with cell elongation and morphogenesis (Derbyshire et al., 2007; Peaucelle et al., 2011; reviewed in Hayashi and Kaida, 2011). Additionally, increased growth in pollen tubes is associated with increased exocytosis of pectins (McKenna et al., 2009), and deficiency in xyloglucans affects various aspects of growth (Cavalier et al., 2008), indicating that the delivery of these components plays an important role in the cell elongation process. Nevertheless, how these cell wall polysaccharides are delivered to the cell wall and which components mediate their secretion are largely unknown. Therefore, our identification of the role of the ECH/YIP4a/YIP4b complex in TGN-mediated secretion of pectin and hemicellulose provides a foundation for dissecting the molecular mechanisms that underpin polysaccharide secretion to the plant cell wall. Importantly, several hormones (e.g., indole-3-acetic acid, ethylene, and brassinosteroids) are thought to mediate their effects on cell elongation via alteration of cell walls (reviewed in Wolf et al., 2012). Thus, identification of components such as ECH and YIP4 in mediating the secretion of cell wall polysaccharides provides an additional control point for the regulation of cell elongation by hormonal and developmental signals.

METHODS

Plant Material

For growth conditions and genotyping of *ech*, see Gendreau et al. (2011). The *Arabidopsis thaliana* (Col-0) T-DNA insertion lines *yip4a-1* (SALK_066428), *yip4a-2* (SALK_021897), and *yip4b* (SALK_129888) were obtained from the SALK Institute. Molecular genotyping was performed using the primers listed in Supplemental Table 1 online.

Transcript levels of the 5' UTR, 3' UTR, and the full-length transcripts of *YIP4a* and *YIP4b* were evaluated using *EF1 α* transcription level as control. PCR reactions were performed on cDNA obtained from leaves (see Supplemental Table 1 online for primers).

The following transgenic fluorescent protein marker lines were used in the Col-0 background: *pRAB-A2a:YFP-RABA2a* (Chow et al., 2008), *pSYP61:SYP61-CFP* (Robert et al., 2008), *pRABF1:RABF1-GFP* (Goh et al., 2007), *pRABF2b:GFP-RABF2b* (Goh et al., 2007), *pVHA-a3:VHA-a3-GFP* (Dettmer et al., 2006), *pVHA-a1:VHA-a1-GFP* (Dettmer et al., 2006), *p35S:N-ST-YFP* and *p35S:NAG1-EGFP* (Grebe et al., 2003), *p35S: γ -TIP-GFP* (Boursiac et al., 2005), and *p35S:Alu-GFP* (Di Sansebastiano et al., 2001) in the Wassilewskija background. *pECH:ECH-YFP* (Gendreau et al., 2011) is in the *ech* background.

Plasmid Construction and Plant Transformation

In total, 1.8 kb of *YIP4a* and 1.3 kb of *YIP4b* promoters were amplified, as well as 2 kb of the *YIP4a* open reading frame and *YIP4b* coding sequence (see Supplemental Table 1 online for all primers). After digestion, promoters were cloned into the *Bam*HI- and *Ascl*-digested vector pSL34

(Ikeda et al., 2009), and the resulting plasmid was *Spe*I and *Not*I digested to ligate either *YIP4a* or *b*. The promoter:gene construct was isolated by *Bam*HI-*Ascl* digestion and transferred into pGreenII 0229 (Basta resistance). Additionally, the insertion of 3*HA in frame at the N-terminal side of *YIP4a* open reading frame was used by annealing HA forward/HA reverse primers (heating to 96°C in ligase buffer followed by cooling to room temperature). The *Agrobacterium tumefaciens* strain C58C1 was transformed with pGreen *YIP4b:YIP4b* and *YIP4a:HA-YIP4a* and used to transform the *Arabidopsis yip4a yip4b* double mutant by the floral dip method (Clough and Bent, 1998).

Length Measurement

Root and hypocotyl lengths were measured with Image J (Abramoff et al., 2004) on pictures taken at full resolution with a Canon 350D camera.

Colocalization Quantification

Colocalization was performed by assessing the proximity of the geometric centers (centroids) of objects in two different channels within the objective resolution (Boutté et al., 2006). The centroid coordinates were obtained using 3D objects counter in Image J (Bolte and Cordelières, 2006). Four to six cells from each of 10 individual roots were analyzed for quantification.

YIP4b Antibody Production

The first 330 bp of *YIP4b* cDNA was amplified, cloned into pET28a, and overexpressed with a C-terminal HIS tag in *Escherichia coli* (strain Rosetta). Four hours after induction with 1 mM isopropyl β -D-thiogalactopyranoside, the expressed 15-kD protein was extracted, purified twice under native conditions using nickel-nitrilotriacetic acid beads, and dialyzed overnight. The correct band was excised from the gel and used for rabbit inoculation. Antibody production and ELISA testing were performed by Agrisera (Sweden). The YIP4b polyclonal antibody from the final bleed serum was affinity purified using the expressed 330-bp fragment of *YIP4b*. This antibody detected a single 30-kD band on protein gel blots (anti-YIP4b 1:250 followed by anti-rabbit-HRP Bio-Rad 1:10,000) with protein extracts from the wild type, *yip4a-1*, and *yip4a-2*, but no band corresponding to YIP4b was observed with the *yip4b*, *yip4a-1 yip4b*, and *yip4a-2 yip4b* protein extracts (Figure 3B, inset), indicating its specificity for YIP4b.

Confocal Laser Scanning Microscopy and Immunolabeling

Fluorescence signals were viewed under an Axioplan inverted microscope with a Zeiss LSM 780 spectral confocal laser scanning microscope. GFP was detected using a 488-nm laser and 493- to 598-nm emission filter; CFP was detected with a 405-nm laser and 454- to 581-nm emission filter. *Arabidopsis* root whole-mount immunolabeling and drug treatments were performed using the same protocol as previously described (Gendreau et al., 2011) using anti-YIP4b (1:150) and anti-rabbit-CY5 (1:300; Jackson ImmunoResearch) or anti-HA (1:700; Covance) followed by anti-mouse TRITC (1:250; Jackson ImmunoResearch). Cy5 was detected using a 633-nm laser and 638- to 759-nm emission filter followed by anti-mouse antibody conjugated with tetramethylrhodamine isothiocyanate with a 561-nm laser and 569- to 638-nm emission filter. For acidic organelle labeling, seedlings were incubated for 30 min in 50 nM lysotracker red (Invitrogen) and detected using a 561-nm laser and 560- to 700-nm emission filter. FM4-64 (5 μ M) and pretreatment with BFA (50 μ M, 1 h) and Wm (33 μ M, 1 h) were executed as previously described (Gendreau et al., 2011).

For hypocotyl and seed coat immunolabeling, samples were high-pressure frozen, freeze-substituted, and embedded in LR White resin as

previously described (McFarlane et al., 2008). Thick sections (250 nm) were prepared using a Leica Ultracut UCT Ultramicrotome and placed on Teflon-coated glass slides (Electron Microscopy Sciences). The morphology of each sample was surveyed by staining with aqueous 1% Toluidine Blue in 1% sodium borate using a Leica DMR microscope. Unstained sections were processed for immunofluorescence as described (Young et al., 2008) using 1:10 of mouse CCRC-M36 or CCRC-M1 from the Complex Carbohydrate Research Center (University of Georgia; Pattathil et al., 2010) or 1:10 rat LM5 (Jones et al., 1997) or JIM7 (Knox et al., 1990) from Leeds University. Sections were incubated in 1:100 goat-anti-mouse or goat-anti-rat antibody conjugated to Alexa488 (Molecular Probes) and viewed under a Leica DMR microscope equipped with an ebg100 mercury fluorescent source with a 450- to 490-nm band-pass excitation filter, no emission filter, and a QICAM digital camera (QImaging).

Transmission Electron Microscopy

High-pressure freezing of 7-d-old root tips was done using a Leica EM HPM100. See Gendreau et al. (2011) for more details.

Ruthenium Red Staining

Mature seeds were incubated in 0.05 M EDTA for 1 h at room temperature with gentle shaking, followed by 1 h incubation in 0.01% (w/v) aqueous solution of Ruthenium red. Seeds were mounted in water and viewed using a Leica MZ9.5 stereomicroscope coupled to a Leica DC300 camera.

Y2H

Coding sequences of *ECH*, *YIP4a*, and *YIP4b* were amplified from *Arabidopsis* root cDNA (see Supplemental Table 1 online for primers), cloned into pGEM-T, and subcloned in the *EcoRI*- and *XhoI*-digested pEG202 and pJG4-5. Y2H was performed according to the manufacturer's instructions (DupLEX-A; OriGene) with pEG202 Δ SphI, a truncated version of GNOM (GN4-4), and pJG4-5 CYCLOPHILIN5 (C-395) as controls (Grebe et al., 2000).

Co-IP

The cloning procedure was identical to cloning for the Y2H assay. Fragments were introduced into pRT104 (N-terminal fusion with 3*MyC or 3*HA). For the co-IP assay, 5 μ g of *ECH* fused to a Myc-tag and *YIP4a* or *YIP4b* fused to a HA tag were transiently expressed in *Arabidopsis* cell culture protoplasts (Fülöp et al., 2005). Immunocomplexes were captured on Protein G sepharose (GE Healthcare) as described by Cruz-Ramírez et al. (2012). Immunodetection of tagged proteins was performed using monoclonal anti-HA-peroxidase conjugate (clone 3F10; Roche), monoclonal anti-c-Myc (clone 9E10; Covance), and chicken anti-c-Myc (Molecular Probes) antibodies.

FT-IR

Four-day-old seedlings were squashed between two BaF₂ windows and abundantly rinsed in distilled water for 2 min. The samples were then dried on the window at 37°C for 20 min. An area of 50 μ m \times 50 μ m halfway up the hypocotyl, on the side of the central cylinder, was selected for spectra collection. Spectra were collected using a ThermoNicolet Nexus spectrometer with a Continuum microscope accessory. Five hypocotyls were measured for each of the four biological replicate giving a total of 20 spectra collected (see Supplemental Data Set 1 online for normalized spectral data). See Mouille et al. (2003) for further info and Robin et al. (2003) for more info on statistical analysis.

Bioinformatic and Phylogenetic Analysis

Multiple protein sequence alignments for YIP4a and YIP4b were generated with T-coffee (Poirot et al., 2003), using Boxshade for shading. Related proteins from yeast and *Arabidopsis* were aligned using MUSCLE (Edgar, 2004), and a phylogenetic tree was constructed using PhyML (www.phylogeny.fr) (Dereeper et al., 2008, 2010) based on the full protein sequence (for details of the procedure; see Supplemental Data Set 2 online).

Accession Numbers

Sequence data from this article can be found in GenBank/EMBL data libraries under the following accession numbers: *ECH*, At1g09330; *YIP4a*, At2g18840; *YIP4b* At4g30260; *YIP1a*, At2g36300; *YIP1b*, At3g52760; *YIP5a*, At2g39805; *YIP5b*, At3g05280; *YIP5c*, At5g27490; *Sc-YIP1*, YGR172C; *Sc-YIP2*, YPR028W; *Sc-YIP3*, YNL044W; *Sc-YIP4*, YGL198W; *Sc-YIP5*, YGL161C; *VHA-a1*, At2g28520; and *SYP61*, At1g28490.

Supplemental Data

The following materials are available in the online version of this article.

Supplemental Figure 1. YIP4a and YIP4b Belong to a Multigenic Family Encoding Transmembrane Proteins.

Supplemental Figure 2. Characterization of yip4 Single and Double Mutants.

Supplemental Figure 3. YIP4a and YIP4b Are TGN Localized.

Supplemental Figure 4. ECH and YIP4b Are Partially Mislocalized in yip4a yip4b and ech, Respectively.

Supplemental Figure 5. TGN-Golgi Association Is Affected by the Lack of YIP4 Proteins.

Supplemental Figure 6. Endocytic and Vacuolar Routes Are Not Affected in yip4a yip4b.

Supplemental Figure 7. Cell Wall Composition Altered in Etiolated Hypocotyls of ech and yip4a yip4b.

Supplemental Figure 8. PIN2- and PIN3-GFP Intensity at the Plasma Membrane of the Wild Type and yip4a yip4b.

Supplemental Table 1. Sequences of Primers.

Supplemental Data Set 1. FT-IR Normalized Data Used to Create the Dendrogram of Supplemental Figure 7.

Supplemental Data Set 2. Procedure Used for the Phylogenetic Analysis of Supplemental Figure 1.

Supplemental References 1. References for Supplemental Figures.

ACKNOWLEDGMENTS

We thank Natasha Raikhel (SYP61-CFP), Karin Schumacher (VHA-a1 and VHA-a3), Christophe Maurel (γ -TIP), Markus Grebe (C-395, GN4-4, N-ST-YFP, and NAG-EGFP), and Tomohiro Uemura (RabF1-GFP and GFP-RabF2b) for providing published material, the University of British Columbia Bioimaging Facility for technical assistance, and Ingela Sandström for constant help in the lab. We also thank Stephanie Robert and Sebastian Bednarek for helpful comments. This research was funded by a Natural Sciences and Engineering Research Council Discovery Grant to L.S. and by grants from Sveriges lantbruksuniversitet (Excellence), Formas (Funcfiber), and Knut och Alice Wallenbergs Stiftelse Foundations to R.P.B.

AUTHOR CONTRIBUTIONS

D.G., H.E.M., L.S., and R.P.B. designed the research. D.G., H.E.M., G.M., G.L.-T., Y.W., E.J., and J.O. performed research. A.S. contributed new computational tools. D.G., H.E.M., L.S., and R.P.B. analyzed data. D.G., H.E.M., L.S., and R.P.B. wrote the article.

Received April 10, 2013; revised June 13, 2013; accepted June 19, 2013; published July 5, 2013.

REFERENCES

- Abramoff, M.D., Magelhaes, P.J., and Ram, S.J.** (2004). Image Processing with ImageJ. *Biophotonics International* **11**: 36–42.
- Barrowman, J., Wang, W., Zhang, Y., and Ferro-Novick, S.** (2003). The Yip1p.Yip1p complex is required for the fusion competence of endoplasmic reticulum-derived vesicles. *J. Biol. Chem.* **278**: 19878–19884.
- Boite, S., and Cordelières, F.P.** (2006). A guided tour into subcellular colocalization analysis in light microscopy. *J. Microsc.* **224**: 213–232.
- Boite, S., Talbot, C., Boutte, Y., Catrice, O., Read, N.D., and Satiat-Jeuemaitre, B.** (2004). FM-dyes as experimental probes for dissecting vesicle trafficking in living plant cells. *J. Microsc.* **214**: 159–173.
- Boursiac, Y., Chen, S., Luu, D.T., Sorieul, M., van den Dries, N., and Maurel, C.** (2005). Early effects of salinity on water transport in *Arabidopsis* roots. Molecular and cellular features of aquaporin expression. *Plant Physiol.* **139**: 790–805.
- Boutté, Y., Crosnier, M.T., Carraro, N., Traas, J., and Satiat-Jeuemaitre, B.** (2006). The plasma membrane recycling pathway and cell polarity in plants: Studies on PIN proteins. *J. Cell Sci.* **119**: 1255–1265.
- Brüx, A., Liu, T.Y., Krebs, M., Stierhof, Y.D., Lohmann, J.U., Miersch, O., Wasternack, C., and Schumacher, K.** (2008). Reduced V-ATPase activity in the trans-Golgi network causes oxylipin-dependent hypocotyl growth inhibition in *Arabidopsis*. *Plant Cell* **20**: 1088–1100.
- Calero, M., Chen, C.Z., Zhu, W., Winand, N., Havas, K.A., Gilbert, P.M., Burd, C.G., and Collins, R.N.** (2003). Dual prenylation is required for Rab protein localization and function. *Mol. Biol. Cell* **14**: 1852–1867.
- Calero, M., Winand, N.J., and Collins, R.N.** (2002). Identification of the novel proteins Yip4p and Yip5p as Rab GTPase interacting factors. *FEBS Lett.* **515**: 89–98.
- Carpita, N.C.** (2011). Update on mechanisms of plant cell wall biosynthesis: How plants make cellulose and other (1→4)- β -D-glucans. *Plant Physiol.* **155**: 171–184.
- Cavalier, D.M., Lerouxel, O., Neumetzler, L., Yamauchi, K., Reinecke, A., Freshour, G., Zobotina, O.A., Hahn, M.G., Burgert, I., Pauly, M., Raikhel, N.V., and Keegstra, K.** (2008). Disrupting two *Arabidopsis thaliana* xylosyltransferase genes results in plants deficient in xyloglucan, a major primary cell wall component. *Plant Cell* **20**: 1519–1537.
- Chen, C.Z., Calero, M., DeRegis, C.J., Heidtman, M., Barlowe, C., and Collins, R.N.** (2004). Genetic analysis of yeast Yip1p function reveals a requirement for Golgi-localized rab proteins and rab-Guanine nucleotide dissociation inhibitor. *Genetics* **168**: 1827–1841.
- Chen, C.Z., and Collins, R.N.** (2005a). Insights into biological functions across species: Examining the role of Rab proteins in YIP1 family function. *Biochem. Soc. Trans.* **33**: 614–618.
- Chen, C.Z., and Collins, R.N.** (2005b). Analysis and properties of the yeast YIP1 family of Ypt-interacting proteins. *Methods Enzymol.* **403**: 333–339.
- Chevalier, L., Bernard, S., Ramdani, Y., Lamour, R., Bardor, M., Lerouge, P., Follet-Gueye, M.L., and Driouch, A.** (2010). Subcompartment localization of the side chain xyloglucan-synthesizing enzymes within Golgi stacks of tobacco suspension-cultured cells. *Plant J.* **64**: 977–989.
- Chow, C.M., Neto, H., Foucart, C., and Moore, I.** (2008). Rab-A2 and Rab-A3 GTPases define a trans-Golgi endosomal membrane domain in *Arabidopsis* that contributes substantially to the cell plate. *Plant Cell* **20**: 101–123.
- Clough, S.J., and Bent, A.F.** (1998). Floral dip: A simplified method for *Agrobacterium*-mediated transformation of *Arabidopsis thaliana*. *Plant J.* **16**: 735–743.
- Cruz-Ramírez, A., et al.** (2012). A bistable circuit involving SCARECROW-RETINOBLASTOMA integrates cues to inform asymmetric stem cell division. *Cell* **150**: 1002–1015.
- De Matteis, M.A., and Luini, A.** (2008). Exiting the Golgi complex. *Nat. Rev. Mol. Cell Biol.* **9**: 273–284.
- Derbyshire, P., Findlay, K., McCann, M.C., and Roberts, K.** (2007). Cell elongation in *Arabidopsis* hypocotyls involves dynamic changes in cell wall thickness. *J. Exp. Bot.* **58**: 2079–2089.
- Dereeper, A., Audic, S., Claverie, J.M., and Blanc, G.** (2010). BLAST-EXPLORER helps you building datasets for phylogenetic analysis. *BMC Evol. Biol.* **10**: 8.
- Dereeper, A., Guignon, V., Blanc, G., Audic, S., Buffet, S., Chevenet, F., Dufayard, J.F., Guindon, S., Lefort, V., Lescot, M., Claverie, J.M., and Gascuel, O.** (2008). Phylogeny.fr: robust phylogenetic analysis for the non-specialist. *Nucleic Acids Res.* **36** (Web Server issue): W465–W469.
- Dettmer, J., Hong-Hermesdorf, A., Stierhof, Y.D., and Schumacher, K.** (2006). Vacuolar H⁺-ATPase activity is required for endocytic and secretory trafficking in *Arabidopsis*. *Plant Cell* **18**: 715–730.
- Di Sansebastiano, G.P., Paris, N., Marc-Martin, S., and Neuhaus, J.M.** (2001). Regeneration of a lytic central vacuole and of neutral peripheral vacuoles can be visualized by green fluorescent proteins targeted to either type of vacuoles. *Plant Physiol.* **126**: 78–86.
- Drakakaki, G., van de Ven, W., Pan, S., Miao, Y., Wang, J., Keinath, N.K., Weatherly, B., Jiang, L., Schumacher, K., Hicks, G., and Raikhel, N.** (2011). Isolation and proteomic analysis of the SYP61 compartment reveal its role in exocytic trafficking in *Arabidopsis*. *Cell Res.* **22**: 413–424.
- Driouch, A., Follet-Gueye, M.L., Bernard, S., Kousar, S., Chevalier, L., Vitré-Gibouin, M., and Lerouxel, O.** (2012). Golgi-mediated synthesis and secretion of matrix polysaccharides of the primary cell wall of higher plants. *Front. Plant Sci.* **3**: 79.
- Edgar, R.C.** (2004). MUSCLE: Multiple sequence alignment with high accuracy and high throughput. *Nucleic Acids Res.* **32**: 1792–1797.
- Fülöp, K., Pettkó-Szandtner, A., Magyar, Z., Miskolczi, P., Kondoros, E., Dudits, D., and Bakó, L.** (2005). The Medicago CDKC;1-CYCLINT;1 kinase complex phosphorylates the carboxy-terminal domain of RNA polymerase II and promotes transcription. *Plant J.* **42**: 810–820.
- Geldner, N., Anders, N., Wolters, H., Keicher, J., Kornberger, W., Muller, P., Delbarre, A., Ueda, T., Nakano, A., and Jürgens, G.** (2003). The *Arabidopsis* GNOM ARF-GEF mediates endosomal recycling, auxin transport, and auxin-dependent plant growth. *Cell* **112**: 219–230.
- Gendre, D., Oh, J., Boutté, Y., Best, J.G., Samuels, L., Nilsson, R., Uemura, T., Marchant, A., Bennett, M.J., Grebe, M., and Bhalerao, R.P.** (2011). Conserved *Arabidopsis* ECHIDNA protein mediates trans-Golgi-network trafficking and cell elongation. *Proc. Natl. Acad. Sci. USA* **108**: 8048–8053.
- Gendreau, E., Traas, J., Desnos, T., Grandjean, O., Caboche, M., and Höfte, H.** (1997). Cellular basis of hypocotyl growth in *Arabidopsis thaliana*. *Plant Physiol.* **114**: 295–305.
- Goh, T., Uchida, W., Arakawa, S., Ito, E., Dainobu, T., Ebine, K., Takeuchi, M., Sato, K., Ueda, T., and Nakano, A.** (2007). VPS9a,

- the common activator for two distinct types of Rab5 GTPases, is essential for the development of *Arabidopsis thaliana*. *Plant Cell* **19**: 3504–3515.
- Gomez, L., and Chrispeels, M.J.** (1993). Tonoplast and soluble vacuolar proteins are targeted by different mechanisms. *Plant Cell* **5**: 1113–1124.
- Grebe, M., Gadea, J., Steinmann, T., Kientz, M., Rahfeld, J.U., Salchert, K., Koncz, C., and Jürgens, G.** (2000). A conserved domain of the *Arabidopsis* GNOM protein mediates subunit interaction and cyclophilin 5 binding. *Plant Cell* **12**: 343–356.
- Grebe, M., Xu, J., Möbius, W., Ueda, T., Nakano, A., Geuze, H.J., Rook, M.B., and Scheres, B.** (2003). *Arabidopsis* sterol endocytosis involves actin-mediated trafficking via ARA6-positive early endosomes. *Curr. Biol.* **13**: 1378–1387.
- Gutiérrez, R.A., MacIntosh, G.C., and Green, P.J.** (1999). Current perspectives on mRNA stability in plants: Multiple levels and mechanisms of control. *Trends Plant Sci.* **4**: 429–438.
- Hayashi, T., and Kaida, R.** (2011). Functions of xyloglucan in plant cells. *Mol. Plant* **4**: 17–24.
- Heidman, M., Chen, C.Z., Collins, R.N., and Barlowe, C.** (2003). A role for Yip1p in COPII vesicle biogenesis. *J. Cell Biol.* **163**: 57–69.
- Ikeda, Y., Men, S., Fischer, U., Stepanova, A.N., Alonso, J.M., Ljung, K., and Grebe, M.** (2009). Local auxin biosynthesis modulates gradient-directed planar polarity in *Arabidopsis*. *Nat. Cell Biol.* **11**: 731–738.
- Inadome, H., Noda, Y., Kamimura, Y., Adachi, H., and Yoda, K.** (2007). Tvp38, Tvp23, Tvp18 and Tvp15: Novel membrane proteins in the Tlg2-containing Golgi/endosome compartments of *Saccharomyces cerevisiae*. *Exp. Cell Res.* **313**: 688–697.
- Ito, T., Chiba, T., Ozawa, R., Yoshida, M., Hattori, M., and Sakaki, Y.** (2001). A comprehensive two-hybrid analysis to explore the yeast protein interactome. *Proc. Natl. Acad. Sci. USA* **98**: 4569–4574.
- Jackson, C.L., and Casanova, J.E.** (2000). Turning on ARF: The Sec7 family of guanine-nucleotide-exchange factors. *Trends Cell Biol.* **10**: 60–67.
- Jailais, Y., Fobis-Loisy, I., Miège, C., and Gaude, T.** (2008). Evidence for a sorting endosome in *Arabidopsis* root cells. *Plant J.* **53**: 237–247.
- Jin, C., Zhang, Y., Zhu, H., Ahmed, K., Fu, C., and Yao, X.** (2005). Human Yip1A specifies the localization of Yif1 to the Golgi apparatus. *Biochem. Biophys. Res. Commun.* **334**: 16–22.
- Jones, L., Seymour, G.B., and Knox, J.P.** (1997). Localization of pectic galactan in tomato cell walls using a monoclonal antibody specific to (1 \rightarrow 4)-[beta]-D-galactan. *Plant Physiol.* **113**: 1405–1412.
- Kang, B.H.** (2011). Shrinkage and fragmentation of the trans-Golgi network in non-meristematic plant cells. *Plant Signal. Behav.* **6**: 884–886.
- Kang, B.H., Nielsen, E., Preuss, M.L., Mastronarde, D., and Staehelin, L.A.** (2011). Electron tomography of RabA4b- and PI-4K β 1-labeled trans Golgi network compartments in *Arabidopsis*. *Traffic* **12**: 313–329.
- Kano, F., Yamauchi, S., Yoshida, Y., Watanabe-Takahashi, M., Nishikawa, K., Nakamura, N., and Murata, M.** (2009). Yip1A regulates the COPI-independent retrograde transport from the Golgi complex to the ER. *J. Cell Sci.* **122**: 2218–2227.
- Knox, J.P., Linstead, P.J., King, J., Cooper, C., and Roberts, K.** (1990). Pectin esterification is spatially regulated both within cell walls and between developing tissues of root apices. *Planta* **181**: 512–521.
- Lam, S.K., Cai, Y., Tse, Y.C., Wang, J., Law, A.H., Pimpl, P., Chan, H.Y., Xia, J., and Jiang, L.** (2009). BFA-induced compartments from the Golgi apparatus and trans-Golgi network/early endosome are distinct in plant cells. *Plant J.* **60**: 865–881.
- Lynch, M.A., and Staehelin, L.A.** (1992). Domain-specific and cell type-specific localization of two types of cell wall matrix polysaccharides in the clover root tip. *J. Cell Biol.* **118**: 467–479.
- Matern, H., Yang, X., Andrusis, E., Sternglanz, R., Trepte, H.H., and Gallwitz, D.** (2000). A novel Golgi membrane protein is part of a GTPase-binding protein complex involved in vesicle targeting. *EMBO J.* **19**: 4485–4492.
- Matsuoka, K., Bassham, D.C., Raikhel, N.V., and Nakamura, K.** (1995). Different sensitivity to wortmannin of two vacuolar sorting signals indicates the presence of distinct sorting machineries in tobacco cells. *J. Cell Biol.* **130**: 1307–1318.
- McFarlane, H.E., Young, R.E., Wasteney, G.O., and Samuels, A.L.** (2008). Cortical microtubules mark the mucilage secretion domain of the plasma membrane in *Arabidopsis* seed coat cells. *Planta* **227**: 1363–1375.
- McKenna, S.T., Kunkel, J.G., Bosch, M., Rounds, C.M., Vidali, L., Winship, L.J., and Hepler, P.K.** (2009). Exocytosis precedes and predicts the increase in growth in oscillating pollen tubes. *Plant Cell* **21**: 3026–3040.
- Mouille, G., Robin, S., Lecomte, M., Pagant, S., and Höfte, H.** (2003). Classification and identification of *Arabidopsis* cell wall mutants using Fourier-transform infrared (FT-IR) microspectroscopy. *Plant J.* **35**: 393–404.
- Niemes, S., Langhans, M., Viotti, C., Scheuring, D., San Wan Yan, M., Jiang, L., Hillmer, S., Robinson, D.G., and Pimpl, P.** (2010). Retromer recycles vacuolar sorting receptors from the trans-Golgi network. *Plant J.* **61**: 107–121.
- Ortega, J.L., Moguel-Esponda, S., Potenza, C., Conklin, C.F., Quintana, A., and Sengupta-Gopalan, C.** (2006). The 3' untranslated region of a soybean cytosolic glutamine synthetase (GS1) affects transcript stability and protein accumulation in transgenic alfalfa. *Plant J.* **45**: 832–846.
- Pattathil, S., et al.** (2010). A comprehensive toolkit of plant cell wall glycan-directed monoclonal antibodies. *Plant Physiol.* **153**: 514–525.
- Peaucelle, A., Braybrook, S.A., Le Guillou, L., Bron, E., Kuhlemeier, C., and Höfte, H.** (2011). Pectin-induced changes in cell wall mechanics underlie organ initiation in *Arabidopsis*. *Curr. Biol.* **21**: 1720–1726.
- Poirot, O., O'Toole, E., and Notredame, C.** (2003). Tcoffee@igs: A web server for computing, evaluating and combining multiple sequence alignments. *Nucleic Acids Res.* **31**: 3503–3506.
- Richter, S., Voss, U., and Jürgens, G.** (2009). Post-Golgi traffic in plants. *Traffic* **10**: 819–828.
- Robert, S., Chary, S.N., Drakakaki, G., Li, S., Yang, Z., Raikhel, N.V., and Hicks, G.R.** (2008). Endosidin1 defines a compartment involved in endocytosis of the brassinosteroid receptor BRI1 and the auxin transporters PIN2 and AUX1. *Proc. Natl. Acad. Sci. USA* **105**: 8464–8469.
- Robin, S., Lecomte, M., Hofte, H., and Mouille, G.** (2003). A procedure for the clustering of cell wall mutants in the model plant *Arabidopsis* based on Fourier-transform infrared (FT-IR) spectroscopy. *J. Appl. Stat.* **30**: 669–681.
- Sandhu, A.P., Randhawa, G.S., and Dhugga, K.S.** (2009). Plant cell wall matrix polysaccharide biosynthesis. *Mol. Plant* **2**: 840–850.
- Satiat-Jeuemaitre, B., Cole, L., Bourett, T., Howard, R., and Hawes, C.** (1996). Brefeldin A effects in plant and fungal cells: Something new about vesicle trafficking? *J. Microsc.* **181**: 162–177.
- Shakoori, A., Fujii, G., Yoshimura, S., Kitamura, M., Nakayama, K., Ito, T., Ohno, H., and Nakamura, N.** (2003). Identification of a five-pass transmembrane protein family localizing in the Golgi apparatus and the ER. *Biochem. Biophys. Res. Commun.* **312**: 850–857.
- Staehelin, L.A., and Kang, B.H.** (2008). Nanoscale architecture of endoplasmic reticulum export sites and of Golgi membranes as determined by electron tomography. *Plant Physiol.* **147**: 1454–1468.

- Stein, I.S., Gottfried, A., Zimmermann, J., and Fischer von Mollard, G.** (2009). TVP23 interacts genetically with the yeast SNARE VT11 and functions in retrograde transport from the early endosome to the late Golgi. *Biochem. J.* **419**: 229–236.
- Tanimoto, K., et al.** (2011). Characterization of YIPF3 and YIPF4, cis-Golgi Localizing Yip domain family proteins. *Cell Struct. Funct.* **36**: 171–185.
- Toyooka, K., Goto, Y., Asatsuma, S., Koizumi, M., Mitsui, T., and Matsuoka, K.** (2009). A mobile secretory vesicle cluster involved in mass transport from the Golgi to the plant cell exterior. *Plant Cell* **21**: 1212–1229.
- Uetz, P., et al.** (2000). A comprehensive analysis of protein-protein interactions in *Saccharomyces cerevisiae*. *Nature* **403**: 623–627.
- Vicré, M., Jauneau, A., Knox, J.P., and Driouich, A.** (1998). Immunolocalization of beta (1-4) and beta-(1-6)-D-galactan epitopes in the cell wall and Golgi stacks of developing flax root tissues. *Protoplasma* **203**: 26–34.
- Viotti, C., et al.** (2010). Endocytic and secretory traffic in *Arabidopsis* merge in the trans-Golgi network/early endosome, an independent and highly dynamic organelle. *Plant Cell* **22**: 1344–1357.
- Wolf, S., Hématy, K., and Höfte, H.** (2012). Growth control and cell wall signaling in plants. *Annu. Rev. Plant Biol.* **63**: 381–407.
- Worden, N., Park, E., and Drakakaki, G.** (2012). Trans-Golgi network: An intersection of trafficking cell wall components. *J. Integr. Plant Biol.* **54**: 875–886.
- Yang, X., Matern, H.T., and Gallwitz, D.** (1998). Specific binding to a novel and essential Golgi membrane protein (Yip1p) functionally links the transport GTPases Ypt1p and Ypt31p. *EMBO J.* **17**: 4954–4963.
- Yoshida, Y., et al.** (2008). YIPF5 and YIF1A recycle between the ER and the Golgi apparatus and are involved in the maintenance of the Golgi structure. *Exp. Cell Res.* **314**: 3427–3443.
- Young, R.E., McFarlane, H.E., Hahn, M.G., Western, T.L., Haughn, G.W., and Samuels, A.L.** (2008). Analysis of the Golgi apparatus in *Arabidopsis* seed coat cells during polarized secretion of pectin-rich mucilage. *Plant Cell* **20**: 1623–1638.
- Zhang, G.F., and Staehelin, L.A.** (1992). Functional compartmentation of the Golgi apparatus of plant cells: Immunocytochemical analysis of high-pressure frozen- and freeze-substituted sycamore maple suspension culture cells. *Plant Physiol.* **99**: 1070–1083.